Acta Pharmaceutica Sinica B 2023;13(2):765−774

Chinese Pharmaceutical Association
Institute of Materia Medica, Chinese Academy of Medical Sciences

Acta Pharmaceutica Sinica B

www.elsevier.com/locate/apsb
www.sciencedirect.com

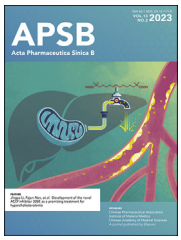

ORIGINAL ARTICLE

Insights into the biosynthesis of septacidin L-heptosamine moiety unveils a VOC family sugar epimerase

Meng Chen[a,b,†], Zhengyan Guo[a,c,†], Jinyuan Sun[a,b,†], Wei Tang[a,b], Min Wang[a,d], Yue Tang[a], Pengwei Li[a], Bian Wu[a,b,*], Yihua Chen[a,b,*]

[a]*State Key Laboratory of Microbial Resources & CAS Key Laboratory of Microbial Physiological and Metabolic Engineering, Institute of Microbiology, Chinese Academy of Sciences, Beijing 100101, China*
[b]*University of Chinese Academy of Sciences, Beijing 100049, China*
[c]*Laboratory of Microbial Metabolic Engineering, Institute of Medicinal Biotechnology, Chinese Academy of Medical Science & Peking Union Medical College, Beijing 100050, China*
[d]*School of Biotechnology and Health Sciences, Wuyi University, Jiangmen 529020, China*

Received 25 March 2022; received in revised form 10 May 2022; accepted 27 May 2022

KEY WORDS

Natural product;
Septacidin;
L-heptose;
Biosynthesis;
Hemiketal;
VOC epimerase;
Catalytic mechanism;
Deprotonation/reprotonation

Abstract L-Heptopyranoses are important components of bacterial polysaccharides and biological active secondary metabolites like septacidin (SEP), which represents a group of nucleoside antibiotics with antitumor, antifungal, and pain-relief activities. However, little is known about the formation mechanisms of those L-heptose moieties. In this study, we deciphered the biosynthetic pathway of the L,L-gluco-heptosamine moiety in SEPs by functional characterizing four genes and proposed that SepI initiates the process by oxidizing the 4′-hydroxyl of L-glycero-α-D-manno-heptose moiety of SEP-328 (**2**) to a keto group. Subsequently, SepJ (C5 epimerase) and SepA (C3 epimerase) shape the 4′-keto-L-heptopyranose moiety by sequential epimerization reactions. At the last step, an aminotransferase SepG installs the 4′-amino group of the L,L-gluco-heptosamine moiety to generate SEP-327 (**3**). An interesting phenomenon is that the SEP intermediates with 4′-keto-L-heptopyranose moieties exist as special bicyclic sugars with hemiacetal-hemiketal structures. Notably, L-pyranose is usually converted from D-pyranose by bifunctional C3/C5 epimerase. SepA is an unprecedented monofunctional L-pyranose C3 epimerase. Further *in silico* and experimental studies revealed that it represents an overlooked metal dependent-sugar epimerase family bearing vicinal oxygen chelate (VOC) architecture.

*Corresponding authors. Tel./fax: +86 10 64806121., +86 10 64806035.
E-mail addresses: wub@im.ac.cn (Bian Wu), chenyihua@im.ac.cn (Yihua Chen).
†These authors made equal contributions to this work.
Peer review under responsibility of Chinese Pharmaceutical Association and Institute of Materia Medica, Chinese Academy of Medical Sciences.

https://doi.org/10.1016/j.apsb.2022.05.031

1. Introduction

Heptoses are important components of bacterial polysaccharides, glycoproteins, and many natural products[1−5]. They play essential roles in immune recognition and virulence of bacteria and biological activities of natural products[6−10]. In recent, heptose-containing bacterial natural products were divided into four groups according to the structures of their seven-carbon sugars[11,12]. Septacidins (SEPs), anicemycin, and spicamycins, the only group of compounds featuring an L-heptosamine moiety, are nucleoside antibiotics consisting of a unique N^6-glycosylated L-heptosamine-adenine core and a side chain with a glycyl-fatty acyl group[11,12]. SEP can act as the inducer of immunogenic cell death and display attractive inhibition activity against skin pathogenic fungi like *Epidermophyton floccosum* and *Trichophyton mentagrophytes*[13−15]. Anicemycin is an inhibitor of anchorage-independent growth of tumor cells[16]. Spicamycin displays excellent antitumor activities and one of its derivatives, KRN5500, entered phase I clinical trial as an anticancer agent and phase II clinical trial as a drug for neuropathic pain relief[17−20].

In previous works, we expressed the *sep* biosynthetic gene cluster in a heterologous host *Streptomyces albus* J1074 to afford *S. albus* 1598 and established that the L-heptose moiety of SEPs is derived from D-sedoheptulose 7-phosphate (S7-P), which is converted to ADP-activated L-glycero-β-D-manno-heptose before the sugar was transferred to the N^6 position of adenine monophosphate (AMP) to form SEP-540 (**1**) (Fig. 1)[11]. A subsequent detachment of the ribosyl-5-phosphate from **1** generates SEP-328 (**2**) with an L-glycero-α-D-manno-heptose (L,D-manno-heptose) moiety[12]. In addition, the *in vivo* studies suggested that SepH is responsible for the attachment of the $N^{4'}$-glycyl group to SEP-327 (**3**) and SepD is the acyltransferase loading the fatty acyl group (Fig. 1)[11]. However, the formation mechanism of the unique structure of SEPs, the 4′-amino-4′-deoxy-L-glycero-β-L-gluco-heptose (L,L-gluco-heptosamine) moiety, remains enigmatic. Actually, although L-heptopyranose moieties spread widely in bacterial surface carbohydrates and some natural products, little is known about their biosynthesis.

In this paper, we delineated the biosynthetic pathway from **2** to **3** and characterized four enzymes that catalyze sequential 4′-oxidation (SepI), 5′-epimerization (SepJ), 3′-epimerization (SepA), and 4′-transamination (SepG) shaping the L,L-gluco-heptosamine moiety. We discovered that the 4′-keto-L-gluco-heptose moieties of SEPs intermediates adopt unusual hemiacetal-hemiketal bicyclic shapes. Further studies revealed that SepA represents an unprecedented vicinal oxygen chelate (VOC) family of sugar epimerases bearing an ion dependent deprotonation/reprotonation catalytic mechanism.

2. Results and discussion

2.1. SepI and SepJ can convert 2 to SEP-326

For the conversion of L,D-manno-heptose to L,L-gluco-heptosamine, two epimerization steps at C3′ and C5′ positions are needed. According to the well elucidated biosynthetic mechanism of L-hexopyranose, 5-epimerization takes place by abstracting a proton from one face of the sugar ring and then replacing it on the other and a 4-keto group is usually introduced to lower the pK_a to facilitate deprotonation[21,22]. In the *sep* gene cluster, we found one putative oxidoreductase gene *sepI*, which encodes a protein belonging to the glucose-methanol-choline (GMC) oxidase/dehydrogenase superfamily[23,24]. Previously, the essential role of *sepI* in SEPs biosynthesis was verified by *in vivo* gene knock-out, and the *S. albus* Δ*sepI* mutant mainly accumulated **2** with the L,D-manno-heptose moiety as a major product[12]. To further probe the function of SepI, N-His$_6$-tagged SepI was expressed in *Escherichia coli* BL21 (DE3) and purified by affinity chromatography (Supporting Information Fig. S1A). When SepI was incubated with **2** and FAD, several product peaks were detected by HPLC and LC−MS (Fig. 2A and Supporting Information Fig. S2B). Subsequent HRMS analyses suggested that all those products had the same molecular formula ($C_{12}H_{15}O_5N_6$), indicating that they were compound **4** and its tautomers (Fig. S2C).

In silico analysis of the *sep* cluster revealed only one putative sugar epimerase gene *sepJ*, which encodes a protein displaying weak homology with the characterized sugar epimerases (*e.g.*, 15% identity with D-tagatose 3-epimerase, GeneBank No. BAA24429.1) of the TIM barrel superfamily[25]. In-frame deletion of *sepJ* blocked the production of SEPs and accumulated **2** in its fermentation broth (Fig. 2B and C), suggesting that SepJ is also involved in the L,L-gluco-heptosamine moiety formation. We expressed N-His$_6$-tagged SepJ in *E. coli* BL21 (DE3) and purified it by affinity chromatography (Fig. S1A). When SepI and SepJ were both added in the assay using **2** as a substrate, SEP-326 (**5**, HRMS, *m/z* 326.1097 $[M+H]^+$), a stable isomer of compound **4**, was generated as a major product (Fig. 2A and Supporting Information Fig. S3B). Compound **4** and its tautomers were also detected as minor products in the SepIJ assay. This assay was then scaled up to prepare enough amount of **5** for structure elucidation. The NMR data supported that **5** contains an adenine and a special N^6-bicyclic L-heptose moiety with a 4′-hemiketal group (Supporting Information Table S1 and Fig. S3). We assumed that SepJ could catalyze the 5′-epimerization of **4** to form **6** with a 4′-keto-L-glycero-β-L-ribo-heptose moiety, which could be converted to **5** *via* a spontaneous nucleophilic attack from the 7′-OH to the 4′-keto group. To check this hypothesis, we incubated **5** in Tris-HCl buffer (pH 8.0) prepared with $H_2^{18}O$ and observed that one ^{18}O atom was efficiently incorporated into this molecule (Supporting Information Fig. S4A). Based on these results, we proposed that **2** was oxidized to compound **4** by SepI, and then epimerized to compound **6** by SepJ, which triggers a spontaneous nucleophilic attack that forms the relatively stable 5 with a bicyclic L-heptose structure. A similar non-enzymatic hemiketal formation was assumed for the tricyclic undecose core of herbicidin, posing another example about polycyclic high-carbon sugar bearing hemiketal structure[26,27].

2.2. SepG is an aminotransferase introducing the 4′-amino group

In silico analysis showed that SepG shares 25.8% identity with DesI, a PLP-dependent aminotransferase involved in desosamine

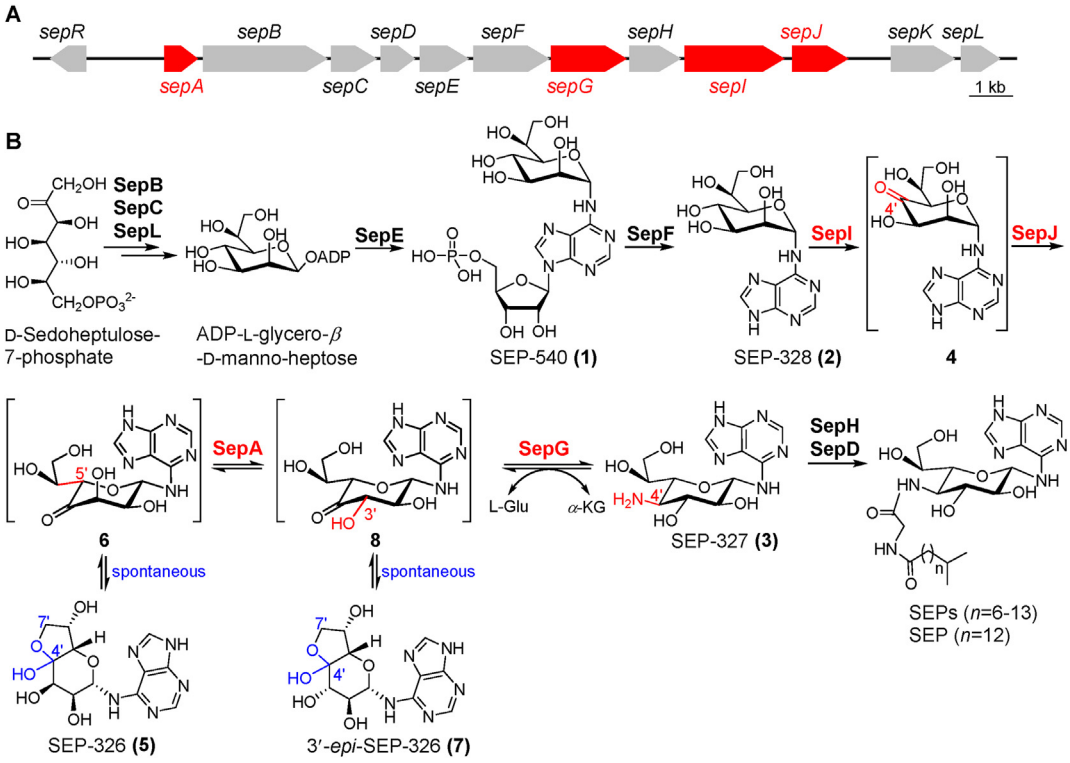

Figure 1 The gene cluster (A) and the proposed biosynthetic pathway (B) of SEPs. Genes studied in this work were indicated in red.

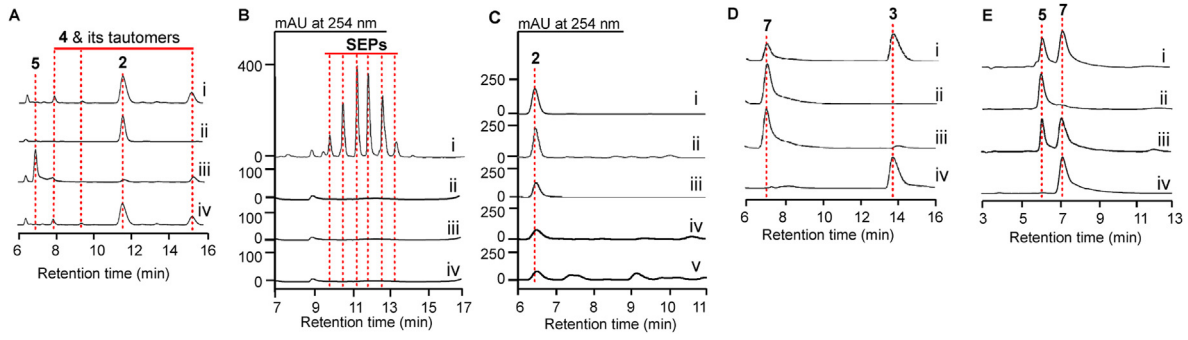

Figure 2 HPLC analyses of the *sep* gene in-frame deletion mutants and the Sep enzyme assays. (A) The SepI and SepIJ assays. i, SepI + **2** + FAD, **4** & its tautomers were detected; ii, SepI (boiled) + **2** + FAD; iii, SepI + SepJ + **2** + FAD, **5** was produced; iv, SepI + **2** + FAD + SepJ (boiled). (B) HPLC profiles of the mycelia methanolic extracts. i, *S. albus* 1598; ii, *S. albus* Δ*sepJ*; iii, *S. albus* Δ*sepG*; iv, *S. albus* Δ*sepA*. (C) HPLC profiles of the fermentation broths of the *sep* gene mutants. i, standard of compound **2**; ii, *S. albus* 1598; iii, *S. albus* Δ*sepJ*; iv, *S. albus* Δ*sepG*; v, *S. albus* Δ*sepA*. (D) The SepG assays. i, SepG + **7** + L-Glu, **3** was produced; ii, SepG (boiled) + **7** + L-Glu; iii, SepG + **3** + α-KG, **7** was produced; iv, SepG (boiled) + **3** + α-KG. (E) The SepA assays. i, SepA + **5**, **7** was produced; ii, SepA (boiled) + **5**; iii, SepA + **7**, **5** was produced; iv, SepA (boiled) + **7**.

biosynthesis[28], and suggested that it is responsible for the incorporation of an amino group to the L,L-gluco-heptosamine moiety. *S. albus* Δ*sepG*, the in-frame deletion mutant of *sepG*, lost the capacity to synthesize SEPs but accumulated **2**, implying the involvement of SepG in the L,L-gluco-heptosamine formation process (Fig. 2B and C). We expressed N-His$_6$-tagged SepG in *E. coli* BL21 (DE3) (Fig. S1A) and studied its catalytic activity by incubating the purified SepG with **3** and α-ketoglutaric acid (α-KG). An efficient conversion of **3** to compound **7** ($C_{12}H_{15}N_5O_6$, *m/z* 326.1100 $[M+H]^+$) with the same molecular formula as **4** and **5** was detected by HPLC and HRMS (Fig. 2D and Supporting Information Fig. S5B). The enzymatic synthesis was then conducted on a preparative scale to obtain enough amount of **7** for NMR analysis and it was determined to be the 3′-epimer of **5** that also possesses a bicyclic L-heptose moiety (Supporting Information Table S2 and Fig. S5). When **7** was incubated in Tris-HCl buffer (pH 8.0) prepared with $H_2^{18}O$, incorporation of one ^{18}O atom into this molecule took place efficiently, suggesting that the real product of the SepG assay was compound **8**, which was converted to **7** *via* a non-enzymatic 4′-hemiketal formation as that for **6** (Fig. S4B). A reverse reaction assay was then set by incubating SepG with **7** and L-glutamic acid (L-Glu), and **3** was produced as anticipated (Fig. 2D), confirming that SepG is responsible for the 4′-keto-L-heptose transamination step.

2.3. *SepA is a L-heptopyranose C3 epimerase*

The structures of **5** and **7** suggest that a 3′-epimerization reaction is needed for SEPs biosynthesis. Till now, no L-pyranose C3 monoepimerase has been discovered. However, there are some bifunctional enzymes possessing L-hexopyranose C3 epimerization activity. GDP-mannose-3′,5′-epimerase (GME) and RmlC are C3/C5 epimerases of GDP-α-D-mannose and TDP-6′-deoxy-α-D-xylo-4′-hexulose, respectively, and they catalyze L-hexose C3 epimerization after D-hexose C5 epimerization[22,29]. CapF and WbvR represent a group of bifunctional enzymes catalyzing UDP-2′-acetamido-2′,6′-dideoxy-4′-keto-β-L-idose C3 epimerization and C4 keto reduction[30,31]. In addition, there are two characterized D-heptose C3 epimerases. Cjj1430 (DdahB) is responsible for sugar C3 epimerization of GDP-4′-keto-6′-deoxy-α-D-lyxo-heptose in *Campylobacter jejuni*[32,33]; AbmJ is a radical SAM protein catalyzing the heptofuranose C3 epimerization in albomycin biosynthesis[34]. However, none of the Sep proteins display considerable similarities with those epimerases.

We noticed that there is still one functional unassigned gene, *sepA*, in the *sep* gene cluster. HPLC analysis of *S. albus* Δ*sepA*, the in-frame deletion mutant of *sepA*, revealed that it lost the capacity to produce SEPs but accumulated **2** in its fermentation broth, implying that SepA participates the L,L-gluco-heptosamine moiety formation (Fig. 2B and C). Therefore, we expressed C-His_6-tagged SepA in *E. coli* BL21 (DE3), purified this protein (Fig. S1A), and incubated it with **5**, which was efficiently converted to **7** by SepA (Fig. 2E). Not surprisingly, SepA could also catalyze the reverse reaction efficiently, supporting its role as L-heptose C3 epimerase.

McCallum et al.[35] proposed that, in *C. jejuni* NCTC 11168, GDP-4′-keto-6′-deoxy-α-D-lyxo-heptose, which is generated from GDP-D-glycero-α-D-manno-heptose by a 4′,6′-dehydration, can be converted to GDP-4′-keto-6′-deoxy-β-L-xylo-heptose by a C3/C5 epimerase Cj1430 (MlghB). An NADPH-dependent ketoreductase Cj1428 (MlghC) then reduces the sugar to GDP-6′-deoxy-β-L-gluco-heptose. In addition, the biosynthesis of GDP-D-glycero-β-L-gluco-heptose in this strain is initiated by Cj1427, which is a sugar 4-oxidase that converts GDP-D-glycero-α-D-manno-heptose to GDP-D-glycero-4′-keto-α-D-lyxo-heptose in the presence of α-KG and NAD^+, and a process analogous to GDP-6′-deoxy-β-L-gluco-heptose formation was assumed for the following reactions affording GDP-D-glycero-β-L-gluco-heptose (Supporting Information Fig. S6)[36,37]. In SEPs biosynthesis, we showed a different way for L-heptose moiety formation. The L,D-manno-heptose of **2** is oxidized by an FAD-dependent 4′-oxidase SepI to generate **4**, which undergoes sequential 5′- and 3′-epimerization reactions that are catalyzed by SepJ (a TIM barrel sugar epimerase) and SepA (an unprecedented monofunctional L-pyranose C3 epimerase), respectively. An aminotransferase SepG then converts the 4′-keto-L-heptose to the L,L-gluco-heptosamine of **3**.

2.4. *Catalytic mechanism of SepA*

As aforementioned, L-pyranose C3 epimerase is very rare, which aroused our interests to investigate the catalytic mechanism of SepA. A further NCBI conserved domain analysis showed that SepA belongs to the VOC family. Proteins in this family are all metalloenzymes with diverse catalytic activities, including extradiol dioxygenases, α-keto acid dependent oxygenase, and isomerases (*e.g.*, methylmalonyl-CoA epimerase and glyoxalase I)[38]. A sequence alignment of SepA with VOC isomerases demonstrated that SepA contains all four conserved residues implicated in the metal active site architecture (Supporting Information Fig. S7). Structure modeling of this protein by AlphaFold showed that the main part of SepA (residue 49 to 160) were folded into two α-helices and eight β-sheets, which formed two structurally equivalent βαββββ domains as observed in many VOC family members (Fig. 3A)[38]. The predicted local Distance Difference Test (plDDT) value of the N-terminal of SepA (residues 1−40) was lower than 50, indicating that it is a disordered region (Supporting Information Fig. S8A and B). We therefore constructed two truncated versions of SepA, $SepA_{30}$ and $SepA_{40}$, with their N-terminal 30 and 40 residues being excised, respectively (Fig. S7). $SepA_{40}$ was easy to denature and precipitate during the purification process and performed a clearly reduced specific activity, while $SepA_{30}$ was stable and showed comparable activity to SepA (Fig. 3D). Therefore, $SepA_{30}$ was used in the following studies. An inductively coupled plasma optical emission spectroscopy (ICP-OES) analysis of $SepA_{30}$ suggested that the metal ion setting in the active site of SepA is manganese (Supporting Information Fig. S9A).

A distance matrix alignment search of $SepA_{30}$ structure against the Protein Data Bank (PDB) was subjected using DALI server and the closest structural homolog was GloA2, a glyoxalase I from *Pseudomonas aeruginosa* PAO1 (PDB ID: 4MTR, z-score = 17.4, identity 28%, and 121 C-α atoms aligned with a RMSD of 1.7 Å) that exists as a homodimer[39]. Since the size-exclusion chromatography suggested a dimeric state of $SepA_{30}$ in solution (Fig. S9B), we assembled $SepA_{30}$ as a homodimer using GloA2 as a template and found that it formed two incompletely closed barrels around the metal ions (Fig. 3A). Unlike some VOC proteins (*e.g.*, methylmalonyl-CoA epimerase) that use one polypeptide to form a barrel structure, $SepA_{30}$ and GloA2 use the βαββββ domains from two different monomers to construct one incompletely closed barrel (Figs. S8C and D)[39,40]. Thus, one active site of $SepA_{30}$ contains four metal binding residues from both chain A (H83 and E129) and chain B (H20 and E67). Subsequently, molecular docking was used to build a model of $SepA_{30}$−**6** complex, in which compound **6** sits snugly in the active site of $SepA_{30}$ (Fig. 3B and C). Its adenine base is anchored by a hydrogen bond between N3 and E113 and the π−π interaction involving Y47, which was supported by the fact that the epimerase activity of both $SepA_{30}$ E113A and Y47A mutants decreased significantly, especially the latter one (Fig. 3D). The L-heptopyranose moiety is oriented by the hydrogen bond interactions from its 3′- and 7′-OH to N131 and the δ-carbonyl group of Q56, respectively, and the 4′-keto group is in the vicinity of the Mn^{2+} ion, which principally serves as an electrophile to anchor the substrate, intermediate and/or transition state in VOC enzymes[38]. Accordingly, both $SepA_{30}$ N131A and Q56A performed reduced epimerase activity, and the $SepA_{30}$ mutants of the metal binding residues (H20A and H83A) exhibited very low catalytic activity (Fig. 3D). Notably, E67 and E129 are both in the vicinity of C3′-H but locate at opposite sides, indicating that they act as acid/base in 3′-epimerization. In consistence with their dual important functions (metal binding and catalysis), both $SepA_{30}$ E67A and E129A substitutions almost abolished the enzyme activity (Fig. 3D).

The $SepA_{30}$ assay was repeated with **5** in deuterated solvent. Incorporation of a single deuterium into **5** ($D_{3'}$-**5**, $C_{12}H_{14}D_1N_5O_6$) and **7** ($D_{3'}$-**7**, $C_{12}H_{14}D_1N_5O_6$) were both observed (Supporting Information Fig. S10), supporting the replacement of a single hydrogen with a deuterium from solvent during the epimerization and a quick equilibrium between the substrate and product. In

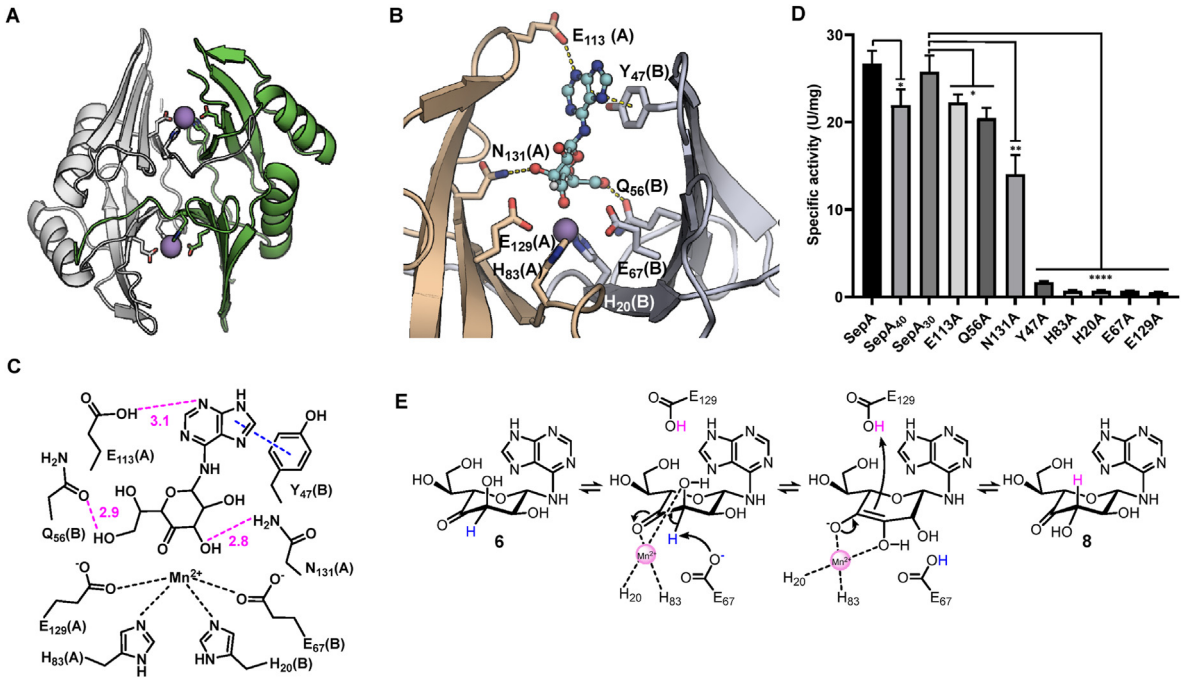

Figure 3 The predicted structure and the catalytic mechanism of SepA. (A) The predicted dimeric structure of $SepA_{30}$. (B) Predicted binding mode of $SepA_{30}$ with **6**. The binding site residues are showed as stick. Residues from chain A or B are indicated in bracket. (C) Schematic representation of the compound **6** binding sites in SepA with labeled interatomic distances (Å). The $\pi-\pi$ interaction, hydrogen bound, and coordinate bond were indicated in blue, magenta, and black, respectively. Residues from chain A or B are indicated in bracket. (D) The specific activities of SepA, $SepA_{40}$, $SepA_{30}$, and its mutants. Data presented as mean ± SD, $n = 3$, *P*-values were calculated using *t* test, $^{****}P < 0.0001$ $^{**}P < 0.01$, $^{*}P < 0.05$. (E) The proposed catalytic mechanism of SepA. For clarity, the coordinate bonds between E67/E129 and Mn^{2+} are not shown.

addition, a coupling $SepA_{30}$/SepG reaction was carried out in D_2O and the resulting double deuterated **3** ($D_{3'}$-$D_{4'}$-**3**, $C_{12}H_{16}D_2N_5O_6$) also supported that one deuterium was incorporated by SepA and the other by SepG (Supporting Information Fig. S11)[28]. Therefore, a deprotonation/reprotonation mechanism was proposed for the SepA catalyzed epimerization, which involves initial proton abstraction from C3′ of **6** by E67, and the forming enolate intermediate is stabilized by the Mn^{2+} center. The following reprotonation proceeds *via* H atom transferring from E129 to the reverse face of C3′ to yield **8** (Fig. 3E). As reported for the other VOC family isomerases, the metal ion ligation in SepA may be sufficient to reduce the pK_a of the C3′ proton of **6** and facilitate its removal[41]. It is distinguished clearly to the L-hexopyranose C3 epimerization catalyzed by NDP-sugar C3/C5 epimerase (GME or RmlC), in which the L-pyranose intermediate adopts a twist boat or an alternate chair form to enable the C3 epimerization by lowering the pK_a of C3 proton[22,29].

2.5. *Distribution of the SepA homologues*

Characterization of SepA discovered an intriguing VOC family sugar epimerase. To investigate the distribution of such sugar epimerases, we searched the NCBI database (till Jan 20, 2022) using SepA as a probe, which resulted in 23 proteins from four orders Streptomycetales (18), Streptosporangiales (3), Micromonosporales (1), and Oscillatoriales (1) with identity and coverage more than 33% and 65%, respectively. Alignment of the SepA homologues revealed that all four residues for metal binding and catalyzing are well conserved (Supporting Information Fig. S12). The SepA homologue proteins were then analyzed phylogenetically along with sugar epimerases from the other five families[21,42], and the epimerases from each family were clustered well except that the TIM barrel ones distributed diffusely. Significantly, SepA and its homologues were clustered in one clade clearly separated from the other families of sugar epimerases (Fig. 4A and Supporting Information Table S3), indicating that the VOC family sugar epimerases have distinctive functions.

We further analyzed the flanking regions of the *sepA* homologues and categorized the 22 gene clusters into three types (Fig. 4B and Supporting Information Table S4). All 12 type I gene clusters (including the *sep* gene cluster) share high level of similarities with the *sep* gene cluster, indicating their products are SEPs analogues. There are 6 type II gene clusters, which contain a gene encoding tridomain NDP-heptose synthetase, implying that they are responsible for heptose-containing compound biosynthesis. Type II gene clusters contain varied number of glycosyltransferase genes. The ones have multiple glycosyltransferase genes may be involved in the assembly of heptose-containing oligosaccharides[43]. In addition, there are two type III gene clusters, which contain genes encoding sugar biosynthesis enzymes and glycosyltransferase but lack heptose related genes, indicating that SepA homologues are not limited to heptose biosynthesis and can be involved in some other sugar metabolisms.

3. Conclusions

By deciphering the biosynthesis of the L,L-gluco-heptosamine moiety of SEPs, we have delineated the whole metabolic pathway that synthesizes SEPs using S-7P, AMP, glycine, and fatty acid as precursors, which sets a solid stage for the following synthetic

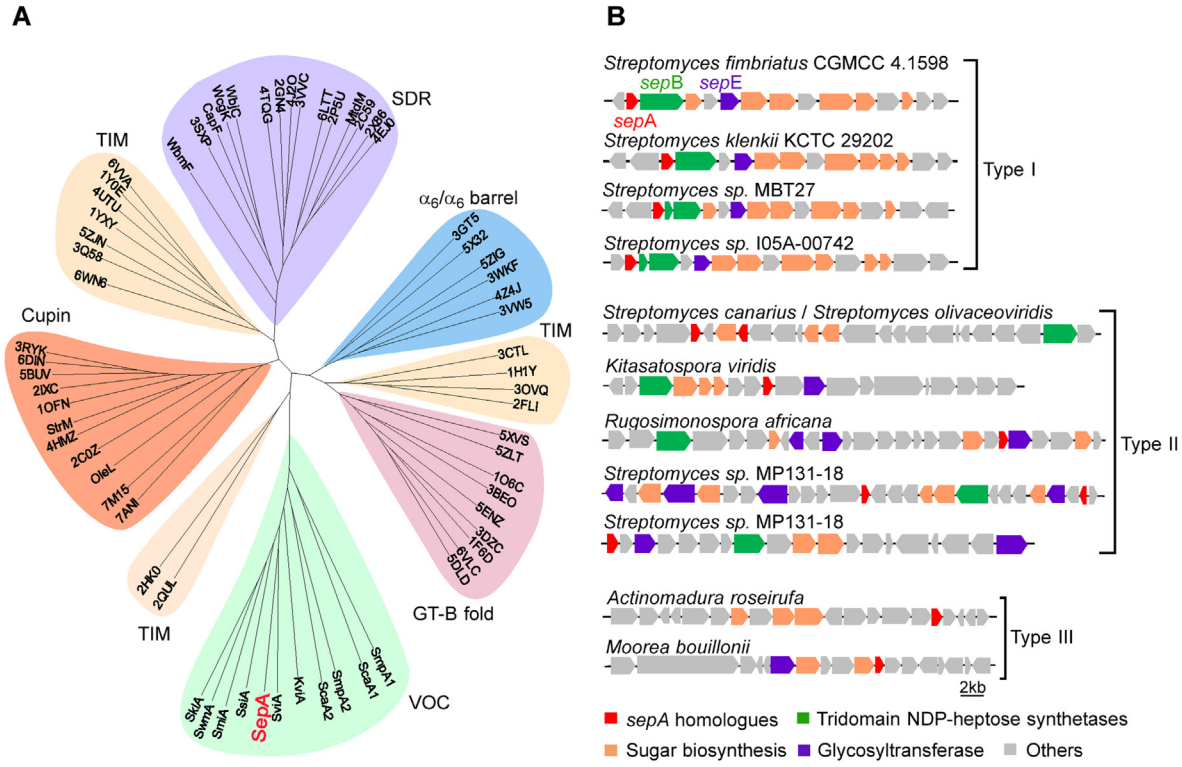

Figure 4 Phylogenetic analysis and distribution of SepA and its homologues. (A) Phylogenetic analysis of sugar epimerases from the VOC family and the other five families (the details of related proteins are listed in Table S3). (B) Schematic representatives of the biosynthetic gene clusters containing genes encoding SepA-like proteins. The *sepA*-like genes were shown in red.

biological and pharmaceutical studies on this group of compounds. In addition, insights into the L,L-gluco-heptosamine moiety biosynthesis revealed some interesting aspects that are distinct to L-hexopyranose formation. In SEPs biosynthesis, the C5 and C3 epimerization steps are catalyzed by two mono-functional enzymes instead of bifunctional enzymes. After C5 epimerization, it was observed that the 4-keto-L-heptopyranose intermediates of SEPs could undergo a non-enzymatic hemiketal formation and existed as relatively stable bicyclic sugars, which may be general to the other L-heptopyranose formation processes. Moreover, we demonstrated that SepA is an unprecedented L-pyranose C3 epimerase representing an overlooked group of VOC family sugar epimerases bearing deprotonation/reprotonation mechanism.

As aforementioned, L-heptopyranose containing natural products, such as septacidins, anicemycins, and spicamycins, exhibit fascinating antifungal, antitumor, and pain relief activities[13−17]. Specifically, KRN5500, a derivative of spicamycin, entered phase I clinical trial as an anticancer agent and phase II trial as a pain relief drug[18−20]. Deciphering the whole biosynthetic process of SEPs, including elucidation of the biosynthesis of the vital L-heptose moiety in this work, lays a solid foundation for the generation of diverse SEP analogues *via* synthetic biological means, which will eventually prompt the development of drugs with L-heptose moieties.

4. Experimental

4.1. DNA manipulation and sequence analysis

DNA manipulations were carried out according to standard procedures[44]. PCRs were performed with Phanta Max Super-Fidelity DNA polymerase (Vazyme) or Taq DNA polymerase (Vazyme) according to the manufacturer's instructions. Strains and plasmids are listed in Supporting Information Table S5. All PCR primers used in this study are listed in Supporting Information Table S6. The λ RED-mediated recombination was performed as described[45]. Isolation of *Streptomyces* genomic DNA and *E. coli*−*Streptomyces* conjugation were carried out according to standard protocols[46,47]. DNA sequencing was performed in GENEWIZ. A BLASTP search was used for functional prediction of proteins (https://blast.ncbi.nlm.nih.gov/Blast.cgi). Multiple alignments were performed with CLUSTALW (https://www.ebi.ac.uk/Tools/msa/clustalw2/). Phylogenetic analysis was performed by MEGA 6.0.

4.2. Construction of the sep gene in-frame deletion mutants

The SEPs heterologous expression strain *S. albus* 1598 was obtained by introducing pSET1598 harboring the whole *sep* cluster captured from *Streptomyces fimbriatus* CGMCC 4.1598 into *S. albus* J1074[11]. The *S. albus* Δ*sepJ*, Δ*sepG*, and Δ*sepA* in-frame deletion mutants were constructed based on *S. albus* 1598 by in-frame gene deletion *via* λ RED-mediated PCR-targeting method. To construct the Δ*sepJ* in-frame deletion mutant, a 1.4-kb *Kan*^{r} cassette flanked with *Spe*I *and Bln*I sites was amplified with primer pair SepJU/SepJD using plasmid pUK-T5promoter as a template and used to replace the *sepJ* gene on pSET1598 *via* λ RED-mediated recombination. The recombinant plasmid was digested with *SpeI/Bln*I to remove the *Kan*^{r} cassette and self-ligated to form plasmid pSET1598-Δ*sepJ* (Supporting Information Fig. S13A). A similar strategy was adopted in the construction of plasmids pSET1598-Δ*sepG* and pSET1598-Δ*sepA* (Figs. S13B and C). The PCR primers for amplifying the

Kan^r cassette that was used in replacement of specific *sep* genes were SepGU/SepGD (*sepG*) and SepAU/SepAD (*sepA*). After verified by sequencing, pSET1598-Δ*sepJ*, pSET1598-Δ*sepG*, *and* pSET1598-Δ*sepA* were introduced into *S. albus* J1074 by *E. coli*−*Streptomyces* conjugation to generate the desired mutant strains *S. albus* Δ*sepJ*, *S. albus* Δ*sepG*, and *S. albus* Δ*sepA*, respectively.

4.3. Production and detection of SEPs in Streptomyces

The *sep* gene cluster heterologous expression strain *S. albus* 1598 and the three mutant strains were grown on MS agar with 50 μg/mL apramycin for sporulation. The collected spore suspension was inoculated into seed medium (1% yeast extract, 1% tryptone, 1% (*v*/*v*) $CoCl_2 \cdot 6H_2O$ solution (0.05%), 0.25% $CaCO_3$, pH 7.3) with 50 μg/mL apramycin and cultured at 28 °C, 220 rpm for 2 days. For production of SEPs, 2 mL seed culture was transferred to 50 mL fermentation medium (1.2% potato starch, 0.8% soybean meal, 0.3% yeast extract, 1% (*v*/*v*) $CoCl_2 \cdot 6H_2O$ solution (0.05%), 0.25% $CaCO_3$, pH 7.3) and cultured at 28 °C, 220 rpm for 5 days.

SEPs and its analogs with fatty acyl decoration are hydrophobic. For their detection, the mycelium was harvested by centrifugation and extract by equal volume of methanol. The extracts were analyzed directly using a ZORBAX CN column (5 μm, 4.6 mm × 250 mm, Agilent Technologies, Santa Clara, USA) on a Shimadzu HPLC system (Shimadzu, Kyoto, Japan), which was developed with solvent A (ddH_2O with 0.1% (*v*/*v*) trifluoroacetic acid) and solvent B (acetonitrile) at a flow rate of 1.0 mL/min. The percentage of solvent B was changed from 30% to 45% over 0−5 min, and from 45% to 53% over 5−21 min. The detection wavelength was 254 nm.

Analyses of the hydrophilic SEPs analogues in supernatants (filtrated with a 0.22 μm membrane) were conducted using a ZORBAX SB-AQ column (5 μm, 4.6 mm × 250 mm, Agilent Technologies, Santa Clara, USA), which was developed with solvent A (ddH_2O with 0.1% (*v*/*v*) trifluoroacetic acid) and solvent B (acetonitrile) at a flow rate of 1.0 mL/min. The percentage of solvent B stayed at 1% over 0−3 min and changed from 1% to 10% over 3−15 min, from 10% to 100% over 15−17 min, and stayed at 100% over 17−19 min. The detection wavelength was 254 nm.

4.4. Expression and purification of SepI, SepJ, SepG, and SepA

The 1.5-kb fragment containing gene *sepI* was amplified with primer pair SepICU/SepICD using *S. fimbriatus* CGMCC 4.1598 genomic DNA as a template. The fragment was verified by sequencing, digested with *Nde*I/*Bam*HI, and then inserted into the same sites of pET28a to generate pET28a-SepI. A single transformant of *E. coli* BL21 (DE3)/pET28a-SepI was pricked and inoculated into LB with 50 μg/mL kanamycin. After cultured overnight at 37 °C, 220 rpm, the broth was used to inoculate LB medium with 50 μg/mL kanamycin at 1:100 dilution and cultured at the same condition until OD_{600} reached 0.6. Expression of SepI was then induced by adding 0.1 mmol/L IPTG and cultured at 16 °C, 180 rpm for further 18−20 h.

The Ni-NTA affinity column was used for N-His_6-tagged SepI purification and all the process were carried out at 4 °C. The cells were harvested by centrifugation and resuspended in binding buffer (20 mmol/L Tris-HCl, 500 mmol/L NaCl, 5 mmol/L imidazole, pH 7.9) for sonication. After removing cell debris by centrifugation at 16,000×*g* for 30 min, the supernatant was loaded onto the Ni-NTA affinity column (well equilibrated with binding buffer). The column was then developed with wash buffer (binding buffer with 60 mmol/L imidazole) and elution buffer (binding buffer with 500 mmol/L imidazole) sequentially and the desired fractions were pooled and desalted with PD-10 column. The purified protein was finally concentrated by ultracentrifugation and stored at −80 °C in 200 mmol/L Tris-HCl (pH 8.0) with 20% glycerol for use. The Bradford assay was adopted for measuring protein concentration using bovine serum albumin as a standard.

For the other three proteins, the 0.9-kb *sepJ* was amplified with primer pair SepJCU/SepJCD using *S. fimbriatus* CGMCC 4.1598 genomic DNA as a template; the 1.3-kb fragment containing gene *sepG* was amplified with primer pair SepGCU/SepGCD; These two fragments were verified by sequencing, digested with *Nde*I/*Bam*HI, and then inserted into the same sites of pET28a individually to afford pET28a-SepJ and pET28a-SepG. The 0.5-kb fragment containing gene *sepA* was amplified with primer pair 22bSepACD/22bSepACU, inserted into the *Nde*I/*Xho*I sites of pET22b, and then transformed to *E. coli* JM109. The colonies grew up on LB agar plate with 100 μg/mL ampicillin were selected and checked by sequencing to select the desired plasmid pET22b-SepA. The expression and purification of N-His_6-tagged SepJ, N-His_6-tagged SepG, and C-His_6-tagged SepA were performed with the same procedures as those for SepI.

4.5. Construction of truncated SepA and its site-directed mutants

The plasmids for expressing $SepA_{40}$ and $SepA_{30}$ were constructed by cloning the N-terminal truncated *sepA* genes with primer pairs 22bSepACU/22bSepA-40D and 22bSepACU/22bSepA-30D from pET22b-SepA and inserting them into the *Nde*I/*Xho*I sites of pET22b, respectively, to generate pET22b-$SepA_{40}$ and pET22b-$SepA_{30}$. Point mutagenesis of $SepA_{30}$ was performed by PCR cloning with primer pairs E67A-F/E67A-R, E129A-F/E129A-R, H20A-F/H20A-R, H83A-F/H83A-R, Y47A-F/Y47A-R, Q56A-F/Q56A-R, E113A-F/E113A-R, and N131A-F/N131A-R using plasmid pET22b-$SepA_{30}$ as a template. After digested with *Dpn*I, the DNAs were purified and transformed to *E. coli* JM109[48]. The colonies that could grow up on LB agar plate with 100 μg/mL ampicillin were picked and the constructs were verified by sequencing to obtain the desired plasmids pET22b-$SepA_{30}$-H20A, pET22b-$SepA_{30}$-E67A, pET22b-$SepA_{30}$-E129A, pET22b-$SepA_{30}$-H83A, pET22b-$SepA_{30}$-Y47A, pET22b-$SepA_{30}$-Q56A, pET22b-$SepA_{30}$-E113A, and pET22b-$SepA_{30}$-N131A. The expression and purification of the truncated and the point mutated proteins were performed with the same procedures as those for $SepA_{30}$.

4.6. SepI and SepJ enzymatic assays

The enzymatic assay of SepI was conducted in a 50 μL mixture containing 200 mmol/L Tris-HCl buffer (pH 8.0), 0.2 mmol/L FAD, 100 mmol/L NaCl, 0.1 mmol/L **2**, and 10 μmol/L SepI at 30 °C for 2 h. The enzymatic assay of SepI and SepJ together was conducted in a 50 μL mixture containing 200 mmol/L Tris-HCl buffer (pH 8.0), 0.2 mmol/L FAD, 0.1 mmol/L **2**, 10 μmol/L SepI, and 5 μmol/L SepJ at 30 °C for 2 h. The reactions were quenched by vibrating with an equal volume of chloroform vigorously[49]. After centrifugation, the upper aqueous phases were analyzed by HPLC using a ZORBAX SB-AQ column (5 μm, 4.6 mm × 250 mm, Agilent Technologies, Santa Clara, USA)

which was developed with solvent A (ddH_2O with 0.1% (*v*/*v*) formic acid) and solvent B (acetonitrile) at a flow rate of 1.0 mL/min. The percentage of solvent B stayed at 1% over 0−16 min and changed from 1% to 100% over 16−18 min. The detection wavelength was 254 nm.

4.7. *SepG enzymatic assay*

The enzymatic assay for the reverse reaction of SepG was carried out in a 50 μL mixture containing 200 mmol/L Tris-HCl buffer (pH 8.0), 100 mmol/L NaCl, 0.5 mmol/L PLP, 0.1 mmol/L **3**, 10 mmol/L α-KG, and 5 μmol/L SepG at 30 °C for 2 h. For probing the transamination activity of SepG, the assay was set in a 50 μL mixture containing 200 mmol/L Tris-HCl buffer (pH 8.0), 100 mmol/L NaCl, 0.5 mmol/L PLP, 0.1 mmol/L **7**, 10 mmol/L L-Glu, and 5 μmol/L SepG at 30 °C for 2 h. The reactions were quenched with chloroform and analyzed by HPLC as that for the SepI and SepJ assays.

4.8. *Enzymatic assays of SepA and its variants*

The enzymatic assay of SepA were carried out in a 50 μL volume mixture containing 200 mmol/L Tris-HCl buffer (pH 8.0), 100 mmol/L NaCl, 0.3 mmol/L **5** or **7** as a substrate, and 1 μmol/L enzyme at 30 °C for 1 h. For detection of the specific activities of SepA, $SepA_{40}$, $SepA_{30}$, and its mutants, the mixture of substrate and buffer was incubated at 30 °C for 15 min. After that, 0.5 μmol/L enzyme was added and the mixture was incubated for another 10 s. The reactions were then quenched with chloroform immediately and analyzed by HPLC as that for the SepI and SepJ assays.

4.9. *Preparation of **5** and **7***

Preparative scale enzymatic reaction of SepIJ was carried out in a 500 μL volume mixture containing 200 mmol/L Tris buffer (pH 8.0, adjusted with HCl), 100 mmol/L NaCl, 20 μmol/L SepI, 10 μmol/L SepJ, 0.2 mmol/L FAD and 1 mmol/L **2** at 30 °C for 3 h. The reaction was quenched by vibrating vigorously with an equal volume of chloroform. After centrifugation, the aqueous phase was subjected to a semi-preparative HPLC (ZORBAX C_{18}, 5 μm, 9.4 mm × 250 mm, Agilent, Santa Clara, USA) eluted with acetonitrile/water (1/99, *v*/*v*) containing 0.1% formic acid at a flow rate of 2.0 mL/min to prepare **5**.

For the preparation of **7**, the enzymatic assay of SepG using **3** as a substrate was carried out in a 500 μL volume mixture containing 200 mmol/L Tris-HCl buffer (pH 8.0, adjusted with HCl), 100 mmol/L NaCl, 0.2 mmol/L PLP, 1 mmol/L **3**, 10 mmol/L α-KG, and 20 μmol/L SepG at 30 °C for 3 h. After quenching with chloroform and centrifugation, **7** was prepared with a same semi-preparative HPLC program as that for **5**.

4.10. *Protein structural prediction and molecular docking study of SepA with **5***

AlphaFold was adopted to predict the structure of SepA and $SepA_{30}$[50]. Homologous sequences of SepA were retrieved from databases (bfd, uniclust30, uniref90, and mgnify) using HHblits or jackhammer with default parameters to build multiple sequence alignment (MSA). Templates were also searched to serve as input of the neural network together with MSA. Five models were generated and relaxed using OpenMM with Amber ff99SB force field. Model ranked first by the neural network was selected for further analysis. Residues at C- and N-terminal with plDDT score lower than 70 were deleted in the final model as developer suggested as low confidence. The structure comparison was performed on DALI server against the Protein Data Bank[51]. Both the assemble patten of the dimer and the position of binding ion was superimposed from the template 4MTR which was co-crystalized with ion Zn^{2+} and replaced with Mn^{2+}. Both receptor and ligand were prepared with AutoDock Tools to add charges for further docking analysis[52,53]. Molecular docking was performed using AutoDock Vina with box size = 20 × 20 × 20. 20 poses were generated and ranked by calculated binding affinities, to investigate the substrate binding mode.

4.11. *Size-exclusion chromatography and metal ion analysis of $SepA_{30}$*

For size-exclusion chromatography analysis, purified recombinant $SepA_{30}$ and molecular weight marker proteins (BSA, ovalbumin, and chymotrypsinogen A) were loaded onto a Superdex 200 16/600 GL column (GE Healthcare) in a 50 mmol/L Tris (pH 7.5) buffer on an ÄKTA Purifier (GE Healthcare). The flow rate was 1 mL/min. Inductively coupled plasma-optical emission spectroscopy (ICP-OES, Optima 5300DV) was used for determining the metal ion in $SepA_{30}$.

4.12. *^{18}O exchange experiments of **5** and **7** in $H_2^{18}O$*

After repeated lyophilization, 0.1 mmol/L **5** or **7** was incubated in 200 mmol/L Tris-HCl buffer (100 mmol/L NaCl, pH 8.0) prepared with $H_2^{18}O$ for 3 h at room temperature. The incorporation of ^{18}O was then analyzed with HR-ESI-MS.

4.13. *Deuterium incorporation experiments*

A sample of deuterated Tris-HCl buffer (200 mmol/L, pH 8.0) and the required compounds (PLP and L-Glu) were prepared by repeated lyophilization and dissolution in an equal volume of D_2O. SepA and SepG were exchanged into deuterated Tris-HCl buffer using Amicon Ultra centrifugal filter devices (Millipore). The SepA reaction was performed in deuterated Tris-HCl buffer (200 mmol/L, pH 8.0), 0.1 mmol/L **5** (dissolved in D_2O), and 1 μmol/L SepA. The SepG reaction was carried out in deuterated Tris-HCl buffer (200 mmol/L, pH 8.0), 0.1 mmol/L **7** (dissolved in D_2O), 5 μmol/L SepG, 0.5 mmol/L PLP, and 10 mmol/L L-Glu. The SepAG reaction was carried out in deuterated Tris-HCl buffer (200 mmol/L, pH 8.0), 0.1 mmol/L **5** (dissolved in D_2O), 1 μmol/L SepA, 5 μmol/L SepG, 0.5 mmol/L PLP, and 10 mmol/L L-Glu. After incubation at 30 °C for 3 h, the enzymes were removed by ultrafiltration (membrane cutoff of 3 kDa). The final samples were lyophilized and dissolved in H_2O three times before LC−MS analysis.[32]

4.14. *Spectroscopic analysis*

HPLC analyses were carried out as described for different compounds. HR-ESI-MS was performed on an Agilent 1260 HPLC/6520 QTOF-MS instrument (Santa Clara, CA, USA) with an electrospray ionization source. NMR analysis was performed at room temperature on a Bruker Advance 500 NMR spectrometer (Billerica, USA).

Compound **5**: white powder; HR-ESI-MS (+) *m*/*z* 326.1097 $[M+H]^+$ (Calcd. for $C_{12}H_{15}N_5O_6$, 326.1095, $[M+H]^+$), see Fig. S3B; ^1H and ^{13}C NMR data, see Table S1; ^1H and ^{13}C NMR

spectra, see Figs. S3C and D; $^{1}H-^{1}H$ COSY, HMQC, HMBC and ROESY spectra, see Supporting Information Fig. S3E–H.

Compound **7**: white powder; HR-ESI-MS (+) *m/z* 326.1100 $[M+H]^+$ (Calcd for $C_{12}H_{15}N_5O_6$, 326.1095, $[M+H]^+$), see Fig. S5B; ^{1}H and ^{13}C NMR data, see Table S2; ^{1}H and ^{13}C NMR spectra, see Fig. S5C and D; $^{1}H-^{1}H$ COSY, HMQC, HMBC and ROESY spectra, see Fig. S5E–H.

Acknowledgments

We thank Dr. Jinwei Ren, Dr. Wenzhao Wang, and Dr. Guomin Ai, Institute of Microbiology, Chinese Academy of Sciences, for technical supports. This study was financially supported by the Ministry of Science and Technology of China (2020YFA0907703) and the National Natural Science Foundation of China (32025002, 31870043).

Author contributions

Yihua Chen and Bian Wu conceived and supervised this project. Meng Chen, Zhengyan Guo and Jinyuan Sun designed and performed experiments. Wei Tang, Min Wang, Yue Tang and Pengwei Li provided resources and critical insights. All authors have given approval to the final version of the manuscript.

Conflicts of interest

The authors declare no conflicts of interest.

Appendix A. Supporting information

Supporting data to this article can be found online at https://doi.org/10.1016/j.apsb.2022.05.031.

References

1. Paulson JC, Blixt O, Collins BE. Sweet spots in functional glycomics. *Nat Chem Biol* 2006;**2**:238–48.
2. Whitfield C, Trent MS. Biosynthesis and export of bacterial lipopolysaccharides. *Annu Rev Biochem* 2014;**83**:99–128.
3. Guerry P, Szymanski CM. Campylobacter sugars sticking out. *Trends Microbiol* 2008;**16**:428–35.
4. Thibodeaux CJ, Melancon 3rd CE, Liu HW. Natural-product sugar biosynthesis and enzymatic glycodiversification. *Angew Chem Int Ed* 2008;**47**:9814–59.
5. Elshahawi SI, Shaaban KA, Kharel MK, Thorson JS. A comprehensive review of glycosylated bacterial natural products. *Chem Soc Rev* 2015;**44**:7591–697.
6. Raetz CRH, Whitfield C. Lipopolysaccharide endotoxins. *Annu Rev Biochem* 2002;**71**:635–700.
7. Hu X, Yang C, Wang PG, Zhang GL. ADP-heptose: a new innate immune modulator. *Carbohydr Res* 2019;**473**:123–8.
8. Yao Q, Lu Q, Wan X, Song F, Xu Y, Hu M, et al. A structural mechanism for bacterial autotransporter glycosylation by a dodecameric heptosyltransferase family. *eLife* 2014;**3**:e03714.
9. Lu Q, Yao Q, Xu Y, Li L, Li S, Liu Y, et al. An iron-containing dodecameric heptosyltransferase family modifies bacterial autotransporters in pathogenesis. *Cell Host Microbe* 2014;**16**:351–63.
10. Guo Z, Tang Y, Tang W, Chen Y. Heptose-containing bacterial natural products: structures, bioactivities, and biosyntheses. *Nat Prod Rep* 2021;**38**:1887–909.
11. Tang W, Guo Z, Cao Z, Wang M, Li P, Meng X, et al. D-Sedoheptulose-7-phosphate is a common precursor for the heptoses of septacidin and hygromycin B. *Proc Natl Acad Sci U S A* 2018;**115**:2818–23.
12. Tang W, Li P, Chen M, Guo Z, Chen Y. Characterization of SepE and SepF for the N^6-glycosylated adenine structure formation in septacidin biosynthesis. *Org Lett* 2020;**22**:5251–4.
13. Dutcher JD, Vonsaltza MH, Pansy FE. Septacidin, a new antitumor and antifungal antibiotic produced by *Streptomyces fibriatus*. *Antimicrob Agents Chemother* 1963;**161**:83–8.
14. Acton EM, Ryan KJ, Luetzow AE. Antitumor septacidin analogues. *J Med Chem* 1977;**20**:1362–71.
15. Sukkurwala AQ, Adjemian S, Senovilla L, Michaud M, Spaggiari S, Vacchelli E, et al. Screening of novel immunogenic cell death inducers within the NCI mechanistic diversity set. *OncoImmunology* 2014;**3**:e28473.
16. Igarashi Y, Ootsu K, Onaka H, Fujita T, Uehara Y, Furumai T. Anicemycin, a new inhibitor of anchorage-independent growth of tumor cells from *Streptomyces* sp. TP-A0648. *J Antibiot* 2005;**58**:322–6.
17. Hayakawa Y, Nakagawa M, Kawai H, Tanabe K, Nakayama H, Shimazu A, et al. Spicamycin, a new differentiation inducer of mouse myeloid leukemia cells (ML) and human promyelocytic leukemia cells (HL-60). *Agric Biol Chem* 1985;**49**:2685–91.
18. Kamishohara M, Kawai H, Sakai T, Isoe T, Hasegawa K, Mochizuki J, et al. Antitumor activity of a spicamycin derivative, KRN5500, and its active metabolite in tumor cells. *Oncol Res* 1994;**6**:383–90.
19. Gadgeel SM, Boinpally RR, Heilbrun LK, Wozniak A, Jain V, Redman B, et al. A phase I clinical trial of spicamycin derivative KRN5500 (NSC 650426) using a phase I accelerated titration "2B" design. *Invest New Drugs* 2003;**21**:63–74.
20. Weinstein SM, Abernethy AP, Spruill SE, Pike IM, True Kelly A, Jett LG. A spicamycin derivative (KRN5500) provides neuropathic pain relief in patients with advanced cancer: a placebo-controlled, proof-of-concept trial. *J Pain Symptom Manage* 2012;**43**:679–93.
21. Van Overtveldt S, Verhaeghe T, Joosten HJ, van den Bergh T, Beerens K, Desmet T. A structural classification of carbohydrate epimerases: from mechanistic insights to practical applications. *Biotechnol Adv* 2015;**33**:1814–28.
22. Major LL, Wolucka BA, Naismith JH. Structure and function of GDP-mannose-3′,5′-epimerase: an enzyme which performs three chemical reactions at the same active site. *J Am Chem Soc* 2005;**127**:18309–20.
23. Cavener DR. GMC oxidoreductases: a newly defined family of homologous proteins with diverse catalytic activities. *J Mol Biol* 1992;**223**:811–4.
24. Aleksenko VA, Anand D, Remeeva A, Nazarenko VV, Gordeliy V, Jaeger KE, et al. Phylogeny and structure of fatty acid photodecarboxylases and glucose-methanol-choline oxidoreductases. *Catalysts* 2020;**10**:1833–40.
25. Yoshida H, Yoshihara A, Ishii T, Izumori K, Kamitori S. X-ray structures of the *Pseudomonas cichorii* D-tagatose 3-epimerase mutant form C66S recognizing deoxy sugars as substrates. *Appl Microbiol Biotechnol* 2016;**100**:10403–15.
26. Lin GM, Romo AJ, Liem PH, Chen Z, Liu HW. Identification and interrogation of the herbicidin biosynthetic gene cluster: first insight into the biosynthesis of a rare undecose nucleoside antibiotic. *J Am Chem Soc* 2017;**139**:16450–3.
27. Pan HX, Chen Z, Zeng T, Jin WB, Geng Y, Lin GM, et al. *Org Lett* 2019;**21**:1374–8.
28. Burgie ES, Holden HM. Molecular architecture of DesI: a key enzyme in the biosynthesis of desosamine. *Biochemistry* 2007;**46**:8999–9006.
29. Dong C, Major LL, Srikannathasan V, Errey JC, Giraud MF, Lam JS, et al. RmlC, a C3′ and C5′ carbohydrate epimerase, appears to operate *via* an intermediate with an unusual twist boat conformation. *J Mol Biol* 2007;**365**:146–59.
30. Knirel YA, Valvano MA. *Bacterial lipopolysaccharides: structure, chemical synthesis, biogenesis and interaction with host cells*. New York: Springer Science & Business Media; 2011.
31. Miyafusa T, Caaveiro JM, Tanaka Y, Tsumoto K. Crystal structure of the enzyme CapF of *Staphylococcus aureus* reveals a unique architecture composed of two functional domains. *Biochem J* 2012;**443**:671–80.

32. Barnawi H, Woodward L, Fava N, Roubakha M, Shaw SD, Kubinec C, et al. Structure-function studies of the C3/C5 epimerases and C4 reductases of the *Campylobacter jejuni* capsular heptose modification pathways. *J Biol Chem* 2021;**296**:100352.
33. McCallum M, Shaw SD, Shaw GS, Creuzenet C. Complete 6-deoxy-D-altro-heptose biosynthesis pathway from *Campylobacter jejuni*: more complex than anticipated. *J Biol Chem* 2012;**287**:29776−88.
34. Ushimaru R, Liu HW. Biosynthetic origin of the atypical stereochemistry in the thioheptose core of albomycin nucleoside antibiotics. *J Am Chem Soc* 2019;**141**:2211−4.
35. McCallum M, Shaw GS, Creuzenet C. Comparison of predicted epimerases and reductases of the *Campylobacter jejuni* d-altro-and l-gluco-heptose synthesis pathways. *J Biol Chem* 2013;**28**:19569−80.
36. Huddleston JP, Anderson TK, Spencer KD, Thoden JB, Raushel FM, Holden HM. Structural analysis of Cj1427, an essential NAD-dependent dehydrogenase for the biosynthesis of the heptose residues in the capsular polysaccharides of *Campylobacter jejuni*. *Biochemistry* 2020;**59**:1314−27.
37. Huddleston JP, Anderson TK, Girardi NM, Thoden JB, Taylor Z, Holden HM, et al. Biosynthesis of D-glycero-l-gluco-heptose in the capsular polysaccharides of *Campylobacter jejuni*. *Biochemistry* 2021; **60**:1552−63.
38. He P, Moran GR. Structural and mechanistic comparisons of the metal-binding members of the vicinal oxygen chelate (VOC) superfamily. *J Inorg Biochem* 2011;**105**:1259−72.
39. Bythell-Douglas R, Suttisansanee U, Flematti GR, Challenor M, Lee M, Panjikar S, et al. The crystal structure of a homodimeric *Pseudomonas* glyoxalase I enzyme reveals asymmetric metallation commensurate with half-of-sites activity. *Chemistry* 2015;**21**: 541−4.
40. McCarthy AA, Baker HM, Shewry SC, Patchett ML, Baker EN. Crystal structure of methylmalonyl-coenzyme A epimerase from *P. Shermanii*: a novel enzymatic function on an ancient metal binding scaffold. *Structure* 2001;**9**:637−46.
41. Himo F, Siegbahn PEM. Catalytic mechanism of glyoxalase I: a theoretical study. *J Am Chem Soc* 2001;**123**:10280−9.
42. Singh S, Phillips Jr GN, Thorson JS. The structural biology of enzymes involved in natural product glycosylation. *Nat Prod Rep* 2012; **29**:1201−37.
43. Tang Y, Tang W, Wang M, Zhang Z, Chen Y. A conservative distribution of tridomain NDP-heptose synthetases in Actinobacteria. *Sci China Life Sci* 2022;**65**:1014−23.
44. Sambrook J, Russell D. *Molecular cloning: a laboratory manual*. Cold Spring Harbor Laboratory; 20011.31−1.162.
45. Gust B, Challis GL, Fowler K, Kieser T, Chater KF. PCR-targeted *streptomyces* gene replacement identifies a protein domain needed for biosynthesis of the sesquiterpene soil odor geosmin. *Proc Natl Acad Sci U S A* 2003;**100**:1541−6.
46. Kieser T, Bibb MJ, Buttner MJ, Chater KF, Hopwood DA. *Practical streptomyces genetics*. Norwich: John Innes Foundation; 2000.
47. Liu N, Guan H, Niu G, Lingjuan J, Li Y, Zhang J, et al. Molecular mechanism of mureidomycin biosynthesis activated by introduction of an exogenous regulatory gene *ssaA* into *Streptomyces roseosporus*. *Sci China Life Sci* 2021;**64**:1949−63.
48. Hu HJ, Wang QQ, Wang DX, Ao YF. Enantioselective biocatalytic desymmetrization for synthesis of enantiopure *cis*-3,4-disubstituted pyrrolidines. *Green Synthesis Catal* 2021;**2**:324−7.
49. Guo Z, Li J, Qin H, Wang M, Lv X, Li X, et al. Biosynthesis of the carbamoylated d-gulosamine moiety of streptothricins: involvement of a guanidino-*N*-glycosyltransferase and an *N*-acetyl-d-gulosamine deacetylase. *Angew Chem Int Ed* 2015;**54**:5175−8.
50. Jumper J, Evans R, Pritzel A, Green T, Figurnov M, Ronneberger O, et al. Highly accurate protein structure prediction with AlphaFold. *Nature* 2021;**596**:583−9.
51. Holm L, Rosenström Pi. Dali server: conservation mapping in 3D. *Nucleic Acids Res* 2010;**38**:545−9.
52. Trott O, Olson AJ. Autodock vina: improving the speed and accuracy of docking with a new scoring function, efficient optimization, and multithreading. *J Comput Chem* 2010;**31**:455−61.
53. Morris GM, Huey R, Lindstrom W, Sanner MF, Belew RK, Goodsell DS, et al. Autodock4 and autodocktools4: automated docking with selective receptor flexibility. *J Comput Chem* 2009;**30**:2785−91.